Chapter 9

Contribution of SAR Radar Images for the Cartography: Case of Mangrove and Post Eruptive Regions

Janvier Fotsing, Emmanuel Tonye, Bernard Essimbi Zobo, Narcisse Talla Tankam and Jean-Paul Rudant

Additional information is available at the end of the chapter

http://dx.doi.org/10.5772/48073

1. Introduction

With the advent of new satellite sensors of type synthetic aperture radar (SAR) (ERS-1 and ERS-2, JERS-1, and RADARSAT), a large number of satellite images are currently available. However, radar remote sensing has a major drawback which is the difficulty to extract the information it contains. Since 1992, several works are conducted with the radar images on Cameroon to study the ecosystem of the coastal zone (Baltzer et al., 1996; Rudant et al., 1997) and the Mount Cameroon region (Akono et al., 2005, 2006; Talla, 2008).

Texture analysis is a robust approach of processing satellite radar images. It is a set of mathematical techniques to quantify the different gray levels present in an image in terms of intensity or roughness and distribution. Several methods of texture analysis exist and can be classified into two broad categories: structural methods and statistical methods (Haralick et al., 1979). Structural methods are used for describing the texture by defining primitives and "rules" of arrangement between them. Statistical methods are used for study the relations between a pixel and its neighborhood. They are defined according to different orders: 1, 2, 3, ...,n. The second order is the most classic, based on co-occurrence matrices. Obtaining these matrices is very time-consuming calculation, which has prompted researchers to not usually go beyond the second order in the evaluation of textural parameters and provides high order information to lower levels (Li, 1994). The matrices of order greater than two are called matrices of frequency. In texture analysis, the interest of researchers is moving increasingly towards optimization methods of evaluation time statistical parameters. Indeed, (Unser, 1995) replaced the co-occurrence matrix by the sum and histograms difference that define the main axes of the probabilities of second order stationary processes.

(Marceau et al., 1990) propose an approach for their textural and spectral classification of different themes and adopt a reduced level of quantification (16, 32 instead of 256). (Peckinpaugh, 1991) for his part describes an efficient approach for calculating texture measures based on co-occurrence matrix, thereby saving valuable time. (Kourgli et al., 1999) present a new algorithm to calculate the statistical parameters of texture through various histograms. Furthermore, Akono et al. (2003) have proposed a new approach in the evaluation of textural parameters of order 3. The present study is a generalization of the work of Akono et al. (2003). It proposes a generic tree method in the evaluation of textural parameters of order $n \geq 2$ near a window image which is to explore as if it were a tree, while memorizing the visited nodes.

Several studies have been conducted in the field of classification by texture analysis. (Ulaby et al., 1986) used texture parameters from the method of co-occurrence to identify four classes of land cover in radar images. (Lucieer et al., 2005) propose a segmentation method based on texture parameters varied for multi object recognition on an image. The authors of this study include an operator called "Local Binary Model," modeling the texture, in a hierarchical segmentation to identify regions with homogeneous texture in an image. In (Linders, 2000), three methods (the method of fuzzy logic, regression analysis and principal component analysis) are used to select significant texture parameters for discrimination of different forest canopies. Recognition of forest cover is then performed by the method of neural networks. Puissant et al. (2005) (Puissant et al., 2005) examine the utility of the textural approach to improve the classification accuracy in an urban context. Texture analysis is compared to multispectral classification. In this study, textural parameters of Haralick (Haralick et al., 1973) of the third order are used. More, (Jukka & Aristide, 1998) have used first-order textural statistics in classifying land used in urban areas by means of Landsat TM and ERS-1. (Franklin & Peddle, 1989) used a mixture of spectral data, topographic (elevation, slope, aspect, curvature, relief) and statistical co-occurrence of the second order for the classification of SPOT images and radar in the boreal. Their work showed that the co-occurrence matrices of second order contain important textural information that improves the discrimination of classes with internal heterogeneity and structural forms. Homogeneous classes of soil are characterized adequately by spectral information alone, but the classes containing mixtures of vegetation types or structural information were characterized more accurately by using a mixture of texture and spectral data. Methods in the literature usually consist create neo-channels of the original image by calculating various parameters of the image texture. The neo-channels created are then combined with each other and the original image, for the production of a classified image. In another study, an analysis of different estimators for the characterization of classes of texture on SAR image is performed (Oliver, 1993). In this study, estimators under the maximum likelihood method are evaluated. Note that this method requires knowledge of the shape of the probability density data to be processed. In (Oliver, 1993), it is also considered a probabilistic description of the texture classes according to the law K and to the Weibull model, which are often applied to characterize classes in SAR images. Other extraction methods of textural parameters have been proposed in the literature (Randen &

Husoy, 1999; Reed & Hans Du Buf, 1993). For most of these methods, a single texture parameter is applied to the discrimination of classes. In this chapter, which applies to images from a radar sensor, we introduce the notions of vector texture, patterns and valleys of the histogram and textural signature for the characterization of classes of land, and show that textural parameters of order higher than 2 are more effective for discrimination of these classes.

In the following, we will present the arborescent method of textural parameters evaluation, followed by the presentation of notion of mode and valley of histogram in SAR image analysis. The criteria of choosing textures parameters are also presented. Once the characterization of the various training zones is done and the classification algorithm is presented. Finally, we present some experimental results.

2. Problem context

The usefulness of image classification is not to be demonstrated today. A good classification requires a better identification of information classes on the image. This identification requires the selection of good feature parameters.

3. Methodology

Our methodology is divided into two parts: the first part concerns the improvement of the computational time required for the evaluation of textural parameters. The second part deals with an approach of SAR images classification.

3.1. Formulation of high order of statistical textural parameters

Basically, statistical textural parameters are function of the occurrence frequency matrix (OFM), which is used to define the occurrence frequency of n-ordered gray levels in the image.

3.1.1. The occurrence frequency matrix (OFM)

In an image with $Ng+1$ levels of quantification, the OFM of order $n>1$ is a $(Ng+1)^n$ size matrix. In this matrix, each element $P_{i_1 i_2 \ldots i_n}$ expresses the occurrence frequency of the n-ordered pixels $(i_0, i_1, \ldots, i_{n-1})$ following the connection rule $R_n(d_1, d_2, \ldots d_{n-1}, \theta_1, \theta_2, \ldots \theta_{n-1})$. This connection rule defines the spatial constraint that must be verified by the various pixels of the n-ordered pixels $(i_0, i_1, \ldots, i_{n-1})$ used in the occurrence frequency matrix evaluation. This rule means that the pixel i_{k+1} $(0<k<n)$ is separated to the pixel i_k by d_{k-1} pixels in the θ_k direction. For the sake of simplicity, $R_n(d_1, d_2, \ldots d_{n-1}, \theta_1, \theta_2, \ldots \theta_{n-1})$ will be noted by R_n in the following.

3.1.2. The textural parameters

A parameter of texture $Para_n$ in any order n is a real function defined in general manner by the equation given after:

$$Para_n = F \times \{R_n\} \to \Re \tag{1}$$

where F is an image or window of image on which one is evaluated texture parameter and R_n is a rule of connection associated.

Let's consider an image window F of size NLxNC, where NL is the number of lines and NC is the number of columns. The classical expression of textural parameters is given by the following expression:

$$Para_n = \sum_{i_0=0}^{N_g} \sum_{i_1=0}^{N_g} \cdots \sum_{i_{n-1}}^{N_g} \left(\phi(i_0, i_1, \cdots, i_{n-1}) \times P_{i_0 i_1 \cdots i_{n-1}} \right) \tag{2}$$

where $\left(P_{i_0 i_1 \cdots i_{n-1}}\right)$ is the OFM and ϕ is a real function defined in N^n.

The synthesis of the generalisation of texture parameters is conciliated on the Table 1 given below.

Parameter		
Order 2	***Classical formulation of order n***	***Arborescent formulation in order n***
1- Contrast		
$\frac{1}{N}\sum_{n=0}^{L-1} n^2 \sum_{i=0}^{L-1}\sum_{j=0}^{L-1}\cdot\left[(i-j)^2 P_{ij}\right]$	$\frac{1}{N}\sum_{i_0=0}^{L-1}\sum_{i_1=0}^{L-1}\cdots\sum_{i_{n-1}=0}^{L-1}\left[n^2\sum_{k=0}^{n-2}\sum_{l=k+1}^{n-1}\left(i_k-i_l\right)^2 P_{i_0 i_1 \cdots i_{n-1}}\right]$	$\frac{1}{N}\sum_{(p,q)\in D}\left[n^2\sum_{u=0}^{n-2}\sum_{l=v+1}^{n-1}\left(i_u-i_v\right)^2\right]$
2- Correlation		
$\frac{1}{N}\sum_{i=0}^{L-1}\sum_{j=0}^{L-1}\cdot\frac{\left(i-\mu_x\right)\left(j-\mu_y\right)}{\sigma_x\sigma_y}P_{ij}$	$\frac{1}{N}\sum_{i_0=0}^{L-1}\sum_{i_1=0}^{L-1}\cdots\sum_{i_{n-1}=0}^{L-1}\left[\frac{\prod_{k=0}^{n-1}\left(i_k-\mu_{i_k}\right)}{\prod_{k=0}^{n-1}\sigma_{i_k}}P_{i_0 i_1 \cdots i_{n-1}}\right]$	$\frac{1}{N}\sum_{(p,q)\in D}\left[\frac{\prod_{u=0}^{n-1}\left(i_u-\mu_{i_u}\right)}{\prod_{u=0}^{n-1}\sigma_{i_u}}\right]$
3- Covariance		
$\frac{1}{N}\sum_{i=0}^{L-1}\sum_{j=0}^{L-1}\cdot\left(i-\mu_x\right)\left(j-\mu_y\right)P_{ij}$	$\frac{1}{N}\sum_{i_0=0}^{L-1}\sum_{i_1=0}^{L-1}\cdots\sum_{i_{n-1}=0}^{L-1}\left[\prod_{k=0}^{n-1}\left(i_k-\mu_{i_k}\right)P_{i_0 i_1 \cdots i_{n-1}}\right]$	$\frac{1}{N}\sum_{(p,q)\in D}\left[\prod_{u=0}^{n-1}\left(i_u-\mu_{i_u}\right)\right]$
4- Inverse Difference		
$\frac{1}{N}\sum_{i=0}^{L-1}\sum_{j=0}^{L-1}\cdot\frac{P_{ij}}{1+\left\|i-j\right\|}$	$\frac{1}{N}\sum_{i_0=0}^{L-1}\sum_{i_1=0}^{L-1}\cdots\sum_{i_{n-1}=0}^{L-1}\left(\frac{P_{i_0 i_1 \cdots i_{n-1}}}{1+\sum_{k=0}^{n-2}\sum_{l=k+1}^{n-1}\left\|i_k-i_l\right\|}\right)$	$\frac{1}{N}\sum_{(p,q)\in D}\left(\frac{1}{1+\sum_{u=0}^{n-2}\sum_{v=u+1}^{n-1}\left\|i_u-i_v\right\|}\right)$
5- Dissymmetry		
$\frac{1}{N}\sum_{i=0}^{L-1}\sum_{j=0}^{L-1}\cdot\left\|i-j\right\|P_{ij}$	$\frac{1}{N}\sum_{i_0=0}^{L-1}\sum_{i_1=0}^{L-1}\cdots\sum_{i_{n-1}=0}^{L-1}\left(\sum_{k=0}^{n-1}\sum_{l=k+1}^{n}\left\|i_k-i_l\right\|P_{i_0 i_1 \cdots i_{n-1}}\right)$	$\frac{1}{N}\sum_{(p,q)\in D}\left(\sum_{u=0}^{n-1}\sum_{v=k+1}^{n}\left\|i_u-i_v\right\|\right)$

6- Standard Deviation		
$\frac{1}{N}\sqrt{\sum_{i=0}^{L-1}\sum_{j=0}^{L-1}(i-\mu_x)^2 P_{ij}}$	$\frac{1}{N}\sqrt{\sum_{i_0=0}^{L-1}\sum_{i_1=0}^{L-1}\cdots\sum_{i_{n-1}=0}^{L-1}\left[(i_0-\mu_x)^2 P_{i_0 i_1\cdots i_{n-1}}\right]}$	$\frac{1}{N}\sqrt{\sum_{(p,q)\in D}(i_0-\mu_x)^2}$
7- Cluster Shade		
$\frac{1}{N}\sum_{i=0}^{L-1}\sum_{j=0}^{L-1}(i+j-2\mu_x)^3 P_{ij}$	$\frac{1}{N}\sum_{i_0=0}^{L-1}\sum_{i_1=0}^{L-1}\cdots\sum_{i_{n-1}=0}^{L-1}\left(\sum_{k=0}^{n-1} i_k - n\mu_x\right)^3 P_{i_0 i_1\cdots i_{n-1}}$	$\frac{1}{N}\left(\sum_{u=0}^{n-1} i_u - n\mu_x\right)^3$
8- Importance of Great Numbers		
$\frac{1}{N}\sum_{i=0}^{L-1}\sum_{j=0}^{L-1}\left(i^2+j^2\right)P_{ij}$	$\frac{1}{N}\sum_{i_0=0}^{L-1}\sum_{i_1=0}^{L-1}\cdots\sum_{i_{n-1}=0}^{L-1}\left[\left(\sum_{k=0}^{n-1}(i_k)^2\right)P_{i_0 i_1\cdots i_{n-1}}\right]$	$\frac{1}{N}\sum_{(p,q)\in D}\left(\sum_{u=0}^{n-1}(i_u)^2\right)$
9- Importance of Small Numbers		
$\frac{1}{N}\sum_{i=0}^{L-1}\sum_{j=0}^{L-1}\frac{P_{ij}}{\left(i^2+j^2\right)+\varepsilon}$	$\frac{1}{N}\sum_{i_0=0}^{L-1}\sum_{i_1=0}^{L-1}\cdots\sum_{i_{n-1}=0}^{L-1}\left(\frac{P_{i_0 i_1\cdots i_{n-1}}}{\sum_{k=0}^{n-1}(i_k)^2+\varepsilon}\right)$	$\frac{1}{N}\sum_{(p,q)\in D}\left(\frac{1}{\sum_{u=0}^{n-1}(i_u)^2+\varepsilon}\right)$
10- Inverse Differential Moment		
$\frac{1}{N}\sqrt{\sum_{i=0}^{L-1}\sum_{j=i+1}^{L-1}\frac{P_{ij}}{1+(i-j)^2}}$	$\frac{1}{N}\sqrt{\sum_{i_0=0}^{L-1}\sum_{i_1=0}^{L-1}\cdots\sum_{i_{n-1}=0}^{L-1}\left(\frac{P_{i_0 i_1\cdots i_{n-1}}}{1+\sum_{k=0}^{n-2}\sum_{l=k+1}^{n-1}(i_k-i_l)^2}\right)}$	$\frac{1}{N}\sum_{(p,q)\in}\left(\frac{1}{1+\sum_{u=0}^{n-2}\sum_{v=u+1}^{n-1}(i_u-i_v)^2}\right)$
11- Mean		
$\frac{1}{N}\sum_{i=0}^{L-1}\sum_{j=0}^{L-1} iP_{ij}$	$\frac{1}{N}\sum_{i_0=0}^{L-1}\sum_{i_1=0}^{L-1}\cdots\sum_{i_{n-1}=0}^{L-1}\left(i_0 P_{i_0 i_1\cdots i_{n-1}}\right)$	$\frac{1}{N}\sum_{(p,q)\in D} i_0$
12- Variance		
$\frac{1}{N}\sum_{i=0}^{L-1}\sum_{j=0}^{L-1}(i-\mu_x)^2 P_{ij}$	$\frac{1}{N}\sum_{i_0=0}^{L-1}\sum_{i_1=0}^{L-1}\cdots\sum_{i_{n-1}=0}^{L-1}\left[(i_0-\mu_x)^2 P_{i_0 i_1\cdots i_{n-1}}\right]$	$\frac{1}{N}\sum_{(p,q)\in D}(i_0-\mu_x)^2$

Table 1. Classical and new formulations of textural parameters of order $n \geq 2$.

3.2. Aborescent method of textural parameters evaluation

This method consists in reducing the number of operations necessary for the calculation of the co-occurrence matrix. From each pixel of the image, all others pixels involved in the computation of the co-occurrence matrix are reached and operations are directly made on these pixels. This process allows avoiding the evaluation and the stocking of the co-occurrence matrix in the main memory of the computer. In the tree approach, the route of the image pixels is not made any more line after line and pixel after pixel, but rather by following a generic tree. From a pixel and according to its position, one reaches directly, by

following a rule of connexion, the neighbouring pixels which are involved in the evaluation of the parameter of texture. After that, the necessary operations are made on these pixels.

3.2.1. Generic tree

The generic tree for the computation of the textural parameters (figure 1) has for seed a pixel positioned in some coordinates (a, b) of the image, with the condition $a \in [0, NL]$ and $b \in [0, NC]$, where NL and NC designate the number of lines and the number of columns of the image, respectively. The different conditions specify the borders of variation of a and b.

From the pixel positioned in coordinates (a, b) of the image window one can reach the pixel positioned in $f_0(a, b, d_1)$ (respectively in $f_1(a, b, d_1)$) by respecting the rule of connexion $R_1(d_1, \theta_1)$ (respectively $R_1(d_1, \theta_1 + 180°)$), if the condition C_0 (respectively the condition C_1) is verified. From the pixel positioned in $f_0(a, b, d_1)$ (respectively in $f_1(a, b, d_1)$) one can reach the pixel positioned in $f_{00}(f_O(a, b, d_1), d_2, \theta_2)$ (respectively in $f_{01}(f_O(a, b, d_1), d_2, \theta_2 + 180°)$) by respecting the rule of connexion $R_2(d_2, \theta_2)$ (respectively $R_2(d_2, \theta_2 + 180°)$), if the condition C_2 (respectively the condition C_3) is verified. Let us call back that a rule of connexion $R_3(d_2, \theta_2)$ means that one considers an inter-pixel distance of d_2 and an angle of θ_2 (and $\theta_2 + 180°$) degrees for the evaluation of the textural parameters. At the order three, one obtains the seven pixels i, j, k, l, m, n, o, presented on the equation 3:

$$\begin{cases} i = (a, b) \\ j = f_0(i, d_1, \theta_1) \\ k = f_{00}(j, d_2, \theta_2) \\ l = f_{01}(j, d_2, \theta_2 + 180°) \\ m = f_1(i, d_1, \theta_1 + 180°) \\ n = f_{10}(m, d_2, \theta_2) \\ o = f_{11}(n, d_2, \theta_2 + 180°) \end{cases} \quad (3)$$

In the equation 3:

i is the current pixel, identified by its coordinates (a, b) in the image;

$f_O(i, d_1, \theta_1)$ is the neighbouring pixel of i respecting the rule of connexion $R_0(d_1, \theta_1)$;

$f_{00}(j, d_2, \theta_2)$ is the neighbouring pixel of j respecting the rule of connexion $R_2(d_2, \theta_2)$;

$f_{01}(j, d_2, \theta_2 + 180°)$ is the neighbouring pixel of j respecting the rule of connexion $R_3(d_2, \theta_2 + 180°)$;

$f_1(i, d_1, \theta_1 + 180°)$ is the neighbouring pixel of i respecting the rule of connexion $R_1(d_1, \theta_1 + 180°)$;

$f_{10}(m, d_2, \theta_2)$ is the neighbouring pixel of m respecting the rule of connexion $R_2(d_2, \theta_2)$;

$f_{11}(n, d_2, \theta_2 + 180°)$ is the neighbouring pixel of m respecting the rule of connexion $R_2(d_2, \theta_2 + 180°)$.

We then generalize by saying that, starting from the pixel $f_n(a, b, d_1, d_2, \cdots, d_n, \theta_n)$, one can reach the pixel $f_{n0}(f_n(a, b, d_1, d_2, \cdots, d_n, \theta_n), d_{n+1}, \theta_{n+1})$(respectively the pixel $f_{n1}(f_n(a, b, d_1, d_2, \cdots, d_n, \theta_n), d_{n+1}, \theta_{n+1} + 180°)$) by respecting the rule of connexion $R_{n0}(d_n, \theta_n)$(respectively the rule of connexion $R_{n1}(d_n, \theta_n + 180°)$), while respecting also the conditions $C_{2^n-1} \cdots C_{2^{n+1}-2}$ for each value of n ($n = 1,2,3, \cdots$). The conditions $C_{2^n-1} \cdots C_{2^{n+1}-2}$ concern the constraints that have to respect $a, b, d_1, d_2, \cdots, d_n$ and the size of the image window. These constraints are major in the processing of the pixels placed in border of the image or in border of the image window. The order of the textural parameter to estimate is the depth of the generic tree. This order is equal here to $n + 1$. On the figure 2, we present the generic for the calculation of textural parameters of order two and on figure 3, we

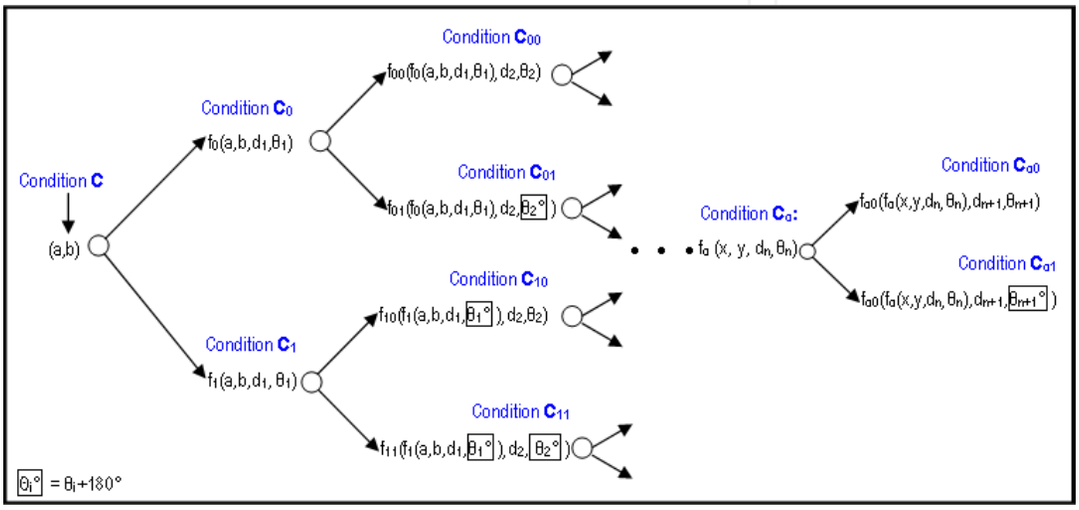

Figure 1. Generic tree for the evaluation of textural parameters of order n>1

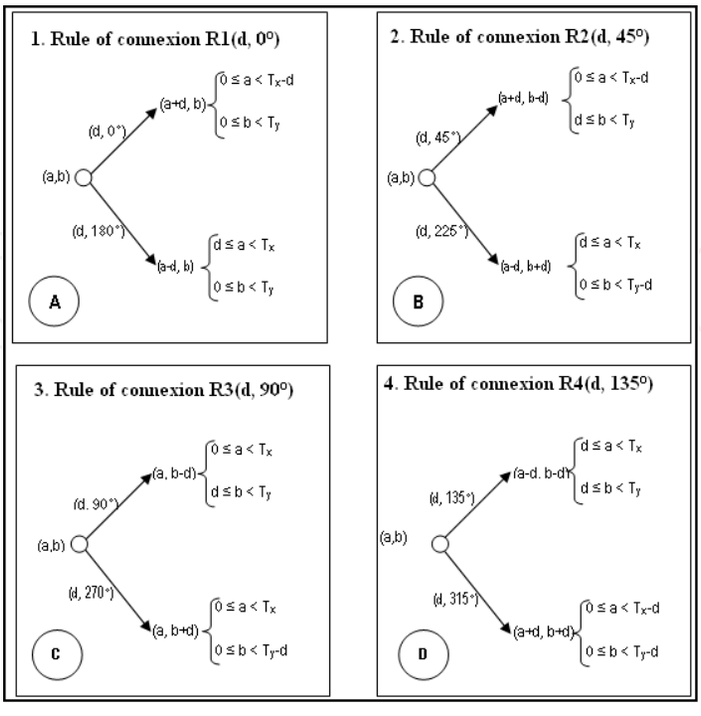

Figure 2. Exploration of the generic tree for the calculation of textural parameters of order two.

present the generic tree for the calculation of textural parameters of order three, for various rules of connexion. The conditions $C_{2^n-1} \cdots C_{2^{n+1}-2}$ are detailed on each of these figures.

- (a, b) is a position of pixel in the image window;
- d is a distance between pixels;
- T_x is a width of window image;
- T_y is a height of window image.

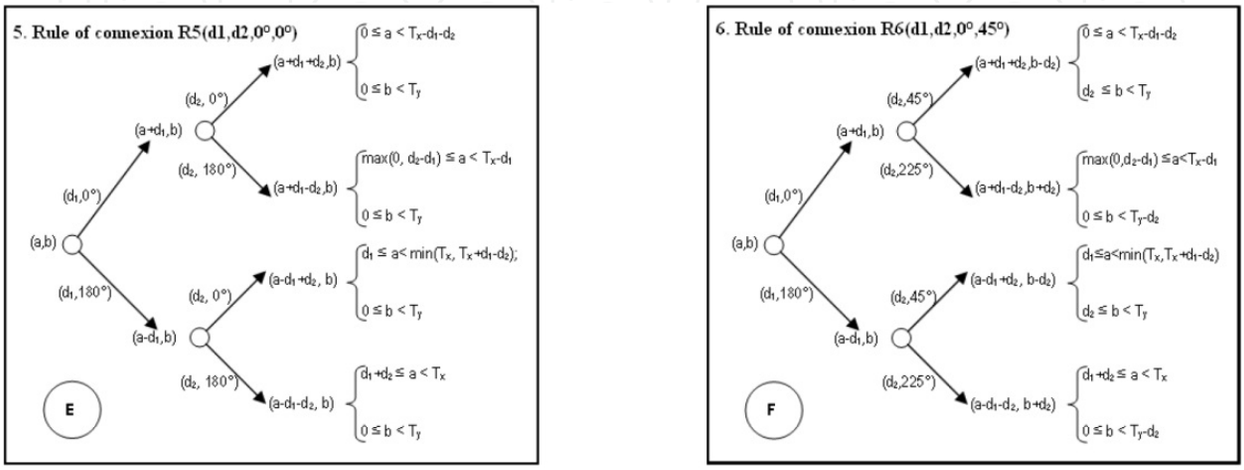

Figure 3. Exploration of the generic tree for the calculation of textural parameters of order three. E : rule of connexion R1 (d1, d2, 0°, 0°) ; F : rule of connexion R2 (d1, d2, 0°, 45°).

3.2.2. Formulation of the textural parameters of order n>1 from the generic tree

On table 1, the expressions of some textural parameters are presented. They are expressed by the approach of generic tree at the order n >1. The corresponding classical formulations are also presented there.

3.2.3. Evaluation of textural parameters from the generic tree

We interest, for example, in the evaluation of the textural parameter «asymmetry» in the order two, in some pixels of an image. The classical formulation of this parameter expresses itself by the equation 4:

$$Asym2 = \sum_{i=0}^{N_g} \sum_{j=0}^{N_g} |i-j| \times p(i,j) \tag{4}$$

In this equation, N_g is the maximal level of gray in the image window and $p(i,j)$ is the occurrence frequency of the pair of levels of gray (i,j) in the image, respecting the rule of connexion $R(d,\theta)$. This parameter can still express itself by the equation 5 :

$$Asym2 = \sum_{i=0}^{N_g} \left(\sum_{j=0}^{N_g} \underbrace{|i-j| + |i-j| + \cdots + |i-j|}_{p(i,j)\ times} \right) \tag{5}$$

The approach using generic tree in this study contains the following stages:

a. create a vector $ASS[N_g + 1]$ (that is a vector of size $N_g + 1$) in a dimension such as the relation below (equation 6) is verified:

$$Asym2 = \sum_{i=0}^{N_g} ASS[i] \tag{6}$$

That means that the vector $ASS[\ ]$ is calculated by the following expression (equation 7):

$$ASS[i] = \sum_{j=0}^{N_g} \left(\underbrace{|i-j| + |i-j| + \cdots + |i-j|}_{p(i,j)\ times} \right); \tag{7}$$

b. initialize the vector $ASS[\ ]$ with 0 (the value 0 is affected in all the entries of the vector);

c. for the entry i of vector $ASS[\ ]$, one adds the value $|i-j|$, provided that pixel j exist and respect the rule of connexion $R(d,\theta)$.

i being pixel in position (a,b) on the generic tree (figure 1), if the condition C_1 (respectively the condition C_2) is verified j will be the pixel in position $f_0(a,b,d_1,\theta_1)$ (respectively in position $f_1(a,b,d_1,\theta_1 + 180°)$). In other words, the entry i of vector $ASS[\ ]$ will be evaluated in the following way (equation 6):

$$ASS[i] = |i - NG(a,b)| + \left|i - NG\left(f_0(a,b,d_1,\theta_1)\right)\right| + \left|i - NG\left(f_1(a,b,d_1,\theta_1 + 180°)\right)\right| \tag{8}$$

$NG(a,b)$, $NG\left(f_0(a,b,d_1,\theta_1)\right)$ and $NG\left(f_1(a,b,d_1,\theta_1 + 180°)\right)$ being levels of gray of the pixels positioned in (a,b), $f_0(a,b,d_1,\theta_1)$ and $f_1(a,b,d_1,\theta_1 + 180°)$ on the generic tree, respectively;

d. repeat the process of stage 3 for all the entries j of the vector $ASS[\ ]$, with $j = 0,1,\cdots,N_g$.

These entries j represent the levels of gray of the pixels being in the considered image window. It is about the image window centered on the current pixel, which is the pixel for which one wants to determine the value of the textural parameter;

e. make the summation of all the elements of the vector $ASS[\ ]$. The result of this summation represents the value of the textural parameter for the current pixel (equation 9):

$$Asym2 = \sum_{j=0}^{N_g} ASS[j]. \tag{9}$$

The results produced by this new approach and those obtained by the classical approach are exactly the same, but the last method requires the evaluation of the co-occurrence matrix, which is very expensive in time of calculation and memory space of the computer. This is due to the fact that the new formulation needs only the evaluation of a one-dimension vector the size of which being equal to a side of the co-occurrence matrix. Furthermore, the evaluation of the co-occurrence matrix makes intervene a lot of operations of multiplication linked in multiple reminders, and these operations are expensive in time machine. It is important to notice that the complexity of calculation increases with the order of the textural parameter.

3.2.4. Example

Let us consider for example the image window below, centered on a pixel having the level of gray 2. Let us estimate the textural parameter «asymmetry» on this window, with the rule of connexion $R(2,45°)$.

0	1	2	4	3
4	0	0	2	3
4	4	**2**	0	1
4	3	2	1	2
4	2	4	4	4

1. Computation by the generic tree approach
   - The maximal level of gray of this image window is 4. A vector $ASS[\ \ ]$ of size 5 is then created and initialized to the value zero.
   - The five following values are calculated: $ASS[O]$, $ASS[1]$, $ASS[2]$, $ASS[3]$ and $ASS[4]$ according to the equation (8), by respecting the rule of connexion $R(2,45°)$ and the neighbouring conditions $C_{2^n-1} \cdots C_{2^{n+1}-2}$, with $n = 1$ (order 2). The following values are then obtained :

$$\begin{cases} ASS[0] = |0-4| + |0-2| = 6 \\ ASS[1] = |1-4| = 3 \\ ASS[2] = |2-4| + |2-3| + |2-4| + |2-3| + |2-3| + |2-0| = 9 \\ ASS[3] = |3-2| + |3-2| + |3-2| = 3 \\ ASS[4] = |4-4| + |4-2| + |4-4| + |4-0| + |4-2| + |4-1| = 11 \end{cases}$$

   - The textural parameter $Asym2$ is equal to the result of the summation of the vector $ASS[\ \ ]$ elements, according to the equation 9. One obtains:

$$Asym2 = ASS[0] + ASS[1] + ASS[2] + ASS[3] + ASS[4] = 32$$

2. Computation with classical approach

Let us make the same calculation by the classical approach of the co-occurrence matrix of levels of gray. In that case the asymmetry is calculated in the considered window by the classical formula: $Asym2 = \sum_{i=0}^{N_g} \sum_{j=0}^{N_g} |i-j| \times P_{ij}$, P_{ij} being the number of time when the pair of levels of gray (i,j) appears in the window, by respecting the rule of connexion $(2,45°)$. The following result is obtained:

$$\begin{aligned} Asym2 = {} & (|0-1| \times P_{01}) + (|0-2| \times P_{02}) + (|0-3| \times P_{03}) + (|0-4| \times P_{04}) \\ & + (|1-0| \times P_{10}) + (|1-2| \times P_{12}) + (|1-3| \times P_{13}) + (|1-4| \times P_{14}) \\ & + (|2-0| \times P_{20}) + (|2-1| \times P_{21}) + (|2-3| \times P_{23}) + (|2-4| \times P_{24}) \\ & + (|3-0| \times P_{30}) + (|3-1| \times P_{31}) + (|3-2| \times P_{32}) + (|3-4| \times P_{34}) \\ & + (|4-0| \times P_{40}) + (|4-1| \times P_{41}) + (|4-2| \times P_{42}) + (|4-3| \times P_{43}) \\ & = [(1 \times 0) + (2 \times 1) + (3 \times 0) + (4 \times 1)] \end{aligned}$$

$$+[(1 \times 0) + (1 \times 0) + (2 \times 0) + (3 \times 1)]$$
$$+[(2 \times 1) + (1 \times 0) + (1 \times 0) + (2 \times 2)]$$
$$+[(3 \times 0) + (2 \times 0) + (1 \times 3) + (1 \times 0)]$$
$$+[(4 \times 1) + (3 \times 1) + (2 \times 2) + (1 \times 0)]$$

$Asym2 = 6 + 3 + 9 + 3 + 11 = 32$

One sees that the result is the same that of the generic tree approach. However, the classical approach is much more complex in the term of calculations.

4. Classification

The methodological approach adopted for the classification consists of four phases: an initial pre-processing of SAR data, a second selection phase of the textural parameters relevant for classification, a third phase mode and valleys selection of the texture image and finally the automatic classification of cluster centers identified on the histogram of image.

4.1. Pre-processing of SAR images

The first phase of treatment consisted of speckle reduction and geometric correction. SAR images are indeed affected by multiplicative noise should be discontinued, or at least reduced to a better interpretation of them (Girard, 2004).The noise is spatially decorrelated from the rest of the image and this is translated by a signal of higher frequency than the image (Pratt, 1991). The Lee filter (Lee, 1981) is applied to reduce speckle (keep low) and improve the readability of structures on the images. This filter preserves the high frequencies (discontinuities) in ERS SAR images (Caloz et al., 2001). Then, the geometric correction of SAR images is performed using topographic map 1: 200000 available on the study site. The radar image is rectified to external data made stackable.

4.2. Analysis and choice of the textural parameters

The notion of the order of statistical texture parameter is very important in matter of analysis of SAR image texture. In fact, the order 2 which is the most classical does not always allow one to identify all the components of a SAR image texture. Above the order 5, Li Wang (1994) proved that the quality of discrimination of the image is deteriorated. Various orders beginning from 2 to 5 will thus enable one to better discriminate a SAR image (Talla, 2003). In fact, experimentally we notice that each order highlight complementary structures to others orders.

Absolutely, there is no universal criterion concerning the selection of texture parameters for image classification. Most often, a succession of texture parameters tests is done and the selection is made empirically. This selection is based on several criterions, notably the capacity of the texture parameter to enhance image discontinuities (Talla et al., 2006a, 2006b), its aptitude to enhance image darkened regions and its aptitude to darken image lit regions. The choice of a parameter is jointly linked to the image itself and the usage.

Experimentally, one parameter has been selected. The mean parameter in order 3 after several tests on our studies site has been selected. The method of choice of the index and order of textural parameters is largely presented in (Fotsing et al., 2008).

4.3. Principle of detection modes and valleys of the histogram

4.3.1. Histogram modeling

The histogram of an image is a graphic representation having abscissa values of gray levels, and the ordinate the number of pixels associated with each gray level value. The mode is a local maximum and valley a local minimum of the histogram. The maximum and minimum (no zero) of a histogram indicate a group of pixels and is used to detect cluster centers. Kourgly et al. (Kourgly et al., 2003) exploit observed nesting on the experimental variogram textures for segmentation urban image.

How to extract the classes contained in a SAR image? A good method for extracting classes is that will arrive at a correct interpretation. To achieve this goal, we used thresholding techniques. We go with the principle that, the thresholding has aim to segment an image in to several classes using only histogram. This assumes that the information associated with the image alone allows the segmentation, which is to say that a class is characterized by its gray level distribution. At each peak of the histogram has an associated class.

There are numerous methods of thresholding a histogram (Diday et al., 1982; Otsu, 1979). Most of these methods are applied correctly if the histogram actually contains separate peaks. Moreover, these methods have often been developed to treat the particular case of segmentation in two classes (that is to say moving to a binary image) and generality face multi-class case is rarely warranty. In this work, we assume that each class corresponds to a different range of gray level. The histogram is then m-modal. The position of minima and maxima of the histogram H can set the thresholds $(m-1)$ to separate the m classes.

In mathematical terms, the thresholds S_i are obtained by equations given below:

$$H(S_i) = Min[H(k)]\ with\ k \in]m_i, m_{i+1}[\tag{10}$$

$$H'(S_i) = Max[H(k)]\ with\ k \in]m_i, m_{i+1}[\tag{11}$$

Equations (10) and (11) indicate the thresholds for valleys and modes of the histogram, respectively. Similarly, in these expressions m_i and m_{i+1} are the mean values (modes or valleys) of the light intensity in the classes C_i and C_{i+1}. The range $]m_i, m_{i+1}[$ is obtained on the basis of average values of the valleys, these when the threshold is calculated by the equation (10) and by (11) otherwise.

The histogram gives comprehensive information on the distribution of gray levels in the image. If we note x the value of gray level, another way to represent the histogram can be to search for a mathematical expression $y = f(x)$ with y the number of pixels whose gray level x. The form of the function f determines the signature of the analyzed image. Based on the

form m-modal histograms in general, we approached a curve of type polynomial regression. These polynomials have formulated by the equation 12:

$$y = a_n x^n + a_{n-1} x^{n-1} + \cdots + a_1 x + a_0 \quad (12)$$

where n is the degree of polynomial.

The continuous function f (the continuous line passing through the vertices of each peak of the histogram) adjusted using the least squares method, allows to set the degree of the number of classes centers.

4.3.2. Determination of degree n

The choice of the number of cluster centers in a radar image is difficult. In his thesis, (Lorette, 1999) uses the entropy criterion for determining the number n of cluster centers for the analysis of urban areas on satellite images.

As part of this project, we used a map of ancient plant formation of the study site. For this, we proposed to re-issue the said card with latest radar image from the perspective of studying the direction of evolution of different forest communities. In general, we decided to use the same number of class with maps of land of the study sites in our possession.

4.3.3. Principle of threshold detection

Detection modes and valleys take place on the transformed histogram, based on the concept of change in concavity of the curve of a function. Indeed, a curve changes concavity through a local minimum (valley) or by a local maximum (mode). The points where the curve changes concavity points are very sensitive and rich in information. The detection of these on the histogram of the transformed SAR image is used to inform the analyzer on the existence of thematic classes. Thematic classes are groups of pixels with similar characteristics (or almost) with respect to their brightness values in the different thematic data. The analyst has the role to determine the usefulness of different thematic classes.

4.3.2.1. Search valleys "inter-modal thresholds"

As part of this work, identification of thresholds is conducted by analyzing the histogram of gray levels and looking for local minima.

Our detection of these thresholds used Fisher's method which uses the criterion of minimizing the sum of the inertia of each class. The calculation algorithm is the dynamic type and evaluating an optimal sequence of partitions according to the scheme described in (Cocquerez et al., 2001).

4.3.2.2. Search modes

We used to detect patterns by Bhattacharya method (Bhattacharya, 1967) that models the histogram by a weighted sum of Gaussian and identifies each mode by its mean and

variance. The algorithm of the method of deployment is widely presented and discussed (Cocquerez et al., 2001).

4.4. Algorithm classification

The final image is classified by the method of detection modes and valleys of the histogram. The classification algorithm implemented is summarized by the following steps:

1. construct the histogram of the image (Table $H[\ ]$);
2. detect n local extrema of Table $H[\ ]$, where n is the number of classes desired. The abscissas of the n local extrema represent the nuclei or centers of different classes of formation;
3. group pixels of the image according to the criterion of minimum distance to the various cluster centers. Each pixel is placed in the class whose center is closest;
4. assign one color to the pixels belonging to the same class and display the resulting image.

The details of the third point of this classification algorithm can be found in (Akono et al., 2003).

5. Application

5.1. Data used

The mangrove is a type of vegetation that grows in water or in mud. We tested the proposed method on a SAR image of E-SAR program (Figure 4), registered on C-band (wavelength 5.66 cm) and VV polarization with a resolution of 6m acquired on the mangrove coastal region of Cameroon.

Figure 4. Experimental image SAR image of the mangrove region

The image obtained from Mount Cameroun region is also used. The studied site is situated in the south west of Cameroon. The Mount Cameroon is a volcano in activity. The image

used (Figure 5) is a SAR image, acquired by ERS-1 satellite in C band (λ = 5.66cm) with VV polarization and SLC (Single Look Complex) format. Its spatial resolution is about 25m and the side of a pixel is 12.5m. This image of 8000 columns and 8269 lines has been acquired on the 7th November 1998.

Due to the lack of a *priori* knowledge on these test sites, various litho-structural maps, formation plant maps including topographic maps and lithographs at 1: 200 000 of scale allowed us to identify the various themes.

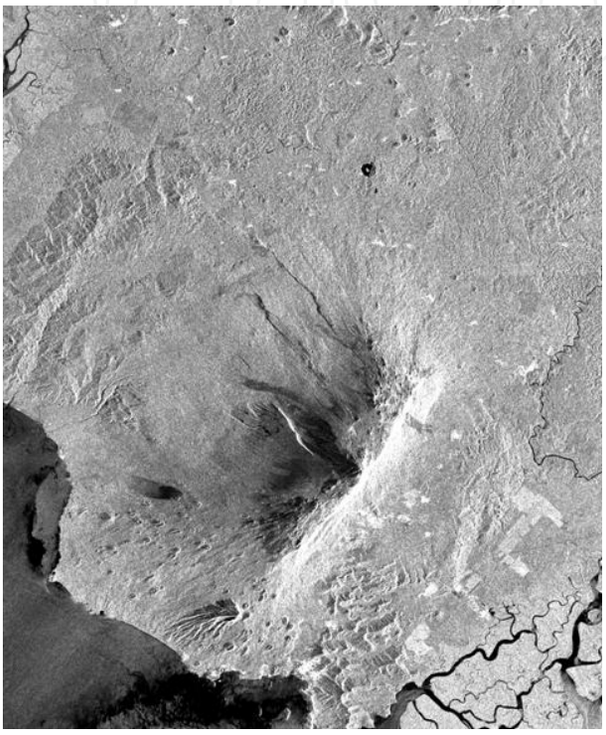

Figure 5. Original image of the Mount Cameroun region

5.2. Histogram and thresholds detection

The histogram of original image of the mangrove region (Figure 4) is illustrated on figure 6. The previous histogram is approximated by the regression curve f which is shown on Figure 7.

The previous approach, which has the advantage of being simple and fast, is well suited to images having forms regularly distributed.

The texture image is obtained from the parameter "Mean" in order 3. The calculation was performed on a window of size 7x7 around each pixel. The choice of this window size is justified by the fact that we get results like the original image with best representation of thematic classes. In addition, we found that the larger of window size was wide, there were more smoothing of the resulting image with absence of fine structure in the image.

The histogram of the texture image is shown in figure 8 and corresponding signature is shown on the figure 9. The irregularities observed on the histogram of texture images

(Figure 8) obtained from the texture index of Haralick introduced on the transformed histogram (Figure 9) many irregularities that can make the fault detection of local minima. This is the main reason that pushed us in this work to adopt a parallel approach to detect patterns of valleys.

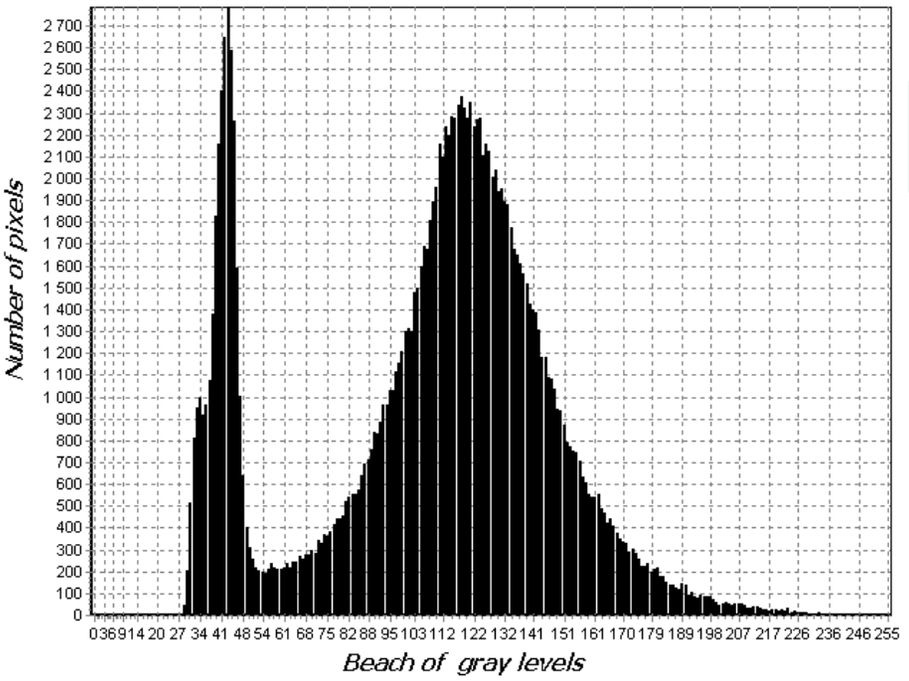

Figure 6. Filtered image histogram illustrating the presence of two classes of intensity in the image of the mangrove region.

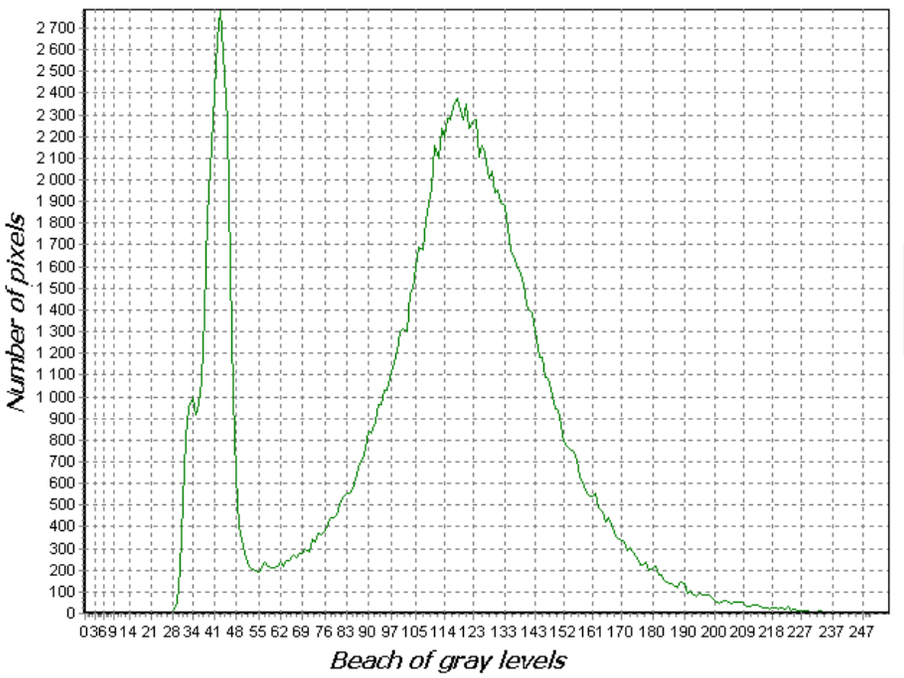

Figure 7. Corresponding signature of the filtered image illustrating the appearance of a polynomial function approximation by the least squares sense.

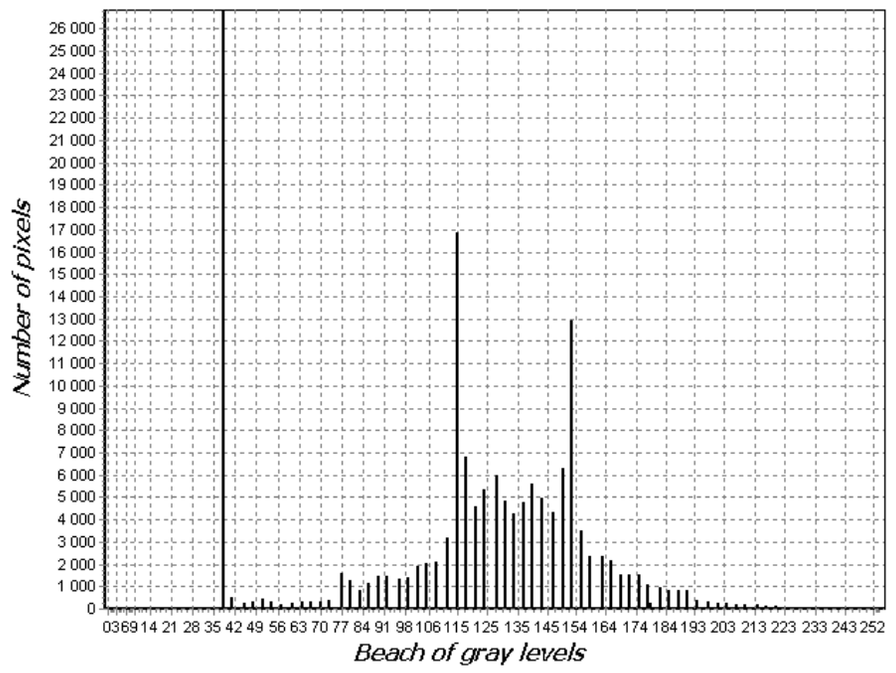

Figure 8. Texture image histogram obtained by index parameter of Haralick "Mean" on the mangrove region

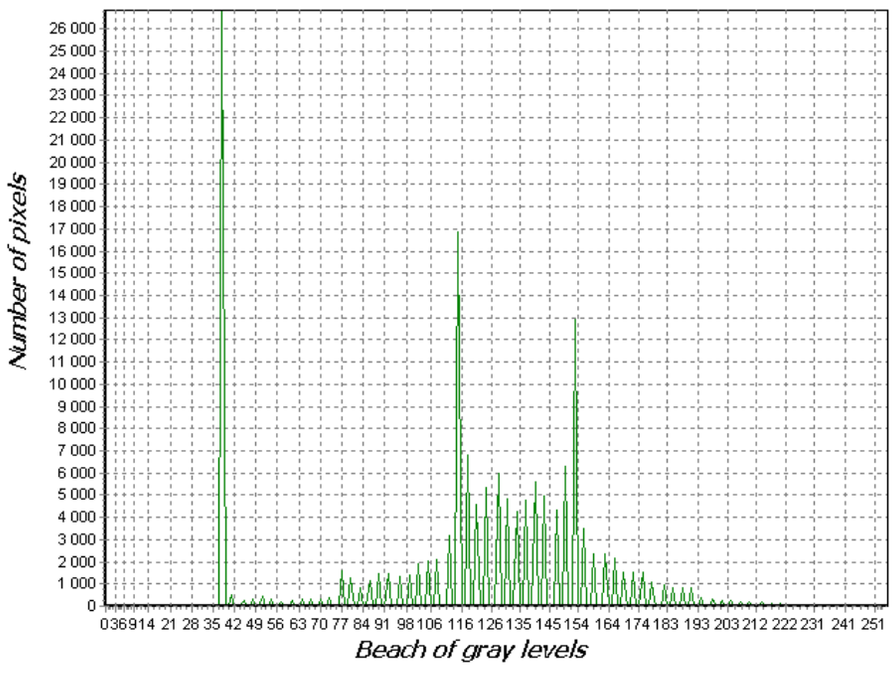

Figure 9. Corresponding signature of the texture image histogram

Table 2 shows the modes and valleys that were used in classification thresholds. It was obtained on the basis of exploitation of the histogram and the signing of the texture image which can be seen representations in figures 8 and 9.

For reference, the histogram of the original image and the texture image obtained on the basis of the radar image taken on the Mount Cameroon region are shown on figures 10 and

11. Signatures (Figures 12 and 13) corresponding to each of the histograms are also immediately followed. It is interesting to note that the texture image was obtained from the parameter "Mean" with a window of size 5x5. These parameters were got after several experimental tests.

	Thresholds / Color codes						
Modes	38	50	76	89	115	153	172
Color codes							
Valleys	45	57	83	96	121	137	179
Color code s							

Table 2. Detection thresholds for classification and color coding of thematic classes: case of mangrove region

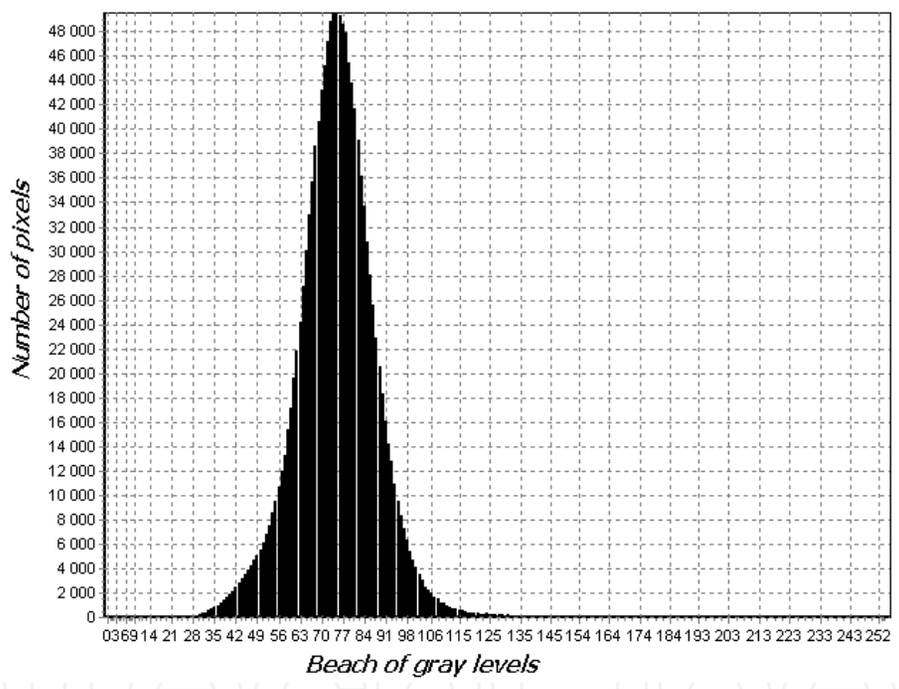

Figure 10. Filtered image histogram illustrating the presence of one main class of intensity in the image of Mount Cameroon region.

It can be seen visually that the histogram of the image filtered even not enough to make a good partition of the base image (Figures 6 and 10). This explains the poor performance of these filters in scenes that contain fine structures such as lineaments, which are generally not well preserved by these filters. Similarly, the histogram of the filtered image does not favor the detection of local extrema accurately. To remedy this shortcoming, a proposal method for modifying the histogram is implemented. It consists of a transformation of the representation of the histogram of the SAR image. For this, a histogram of the envelope curve passing through the ends of each peak is plotted (Figures 7 and 11) using the method of least squares regression. To keep up the properties of both representations, we plan to

keep the same scale in both cases representation. The transformed histogram (Figures 9 and 13) favors the detection of local extrema of peaks from the accentuation of the regression line well represented.

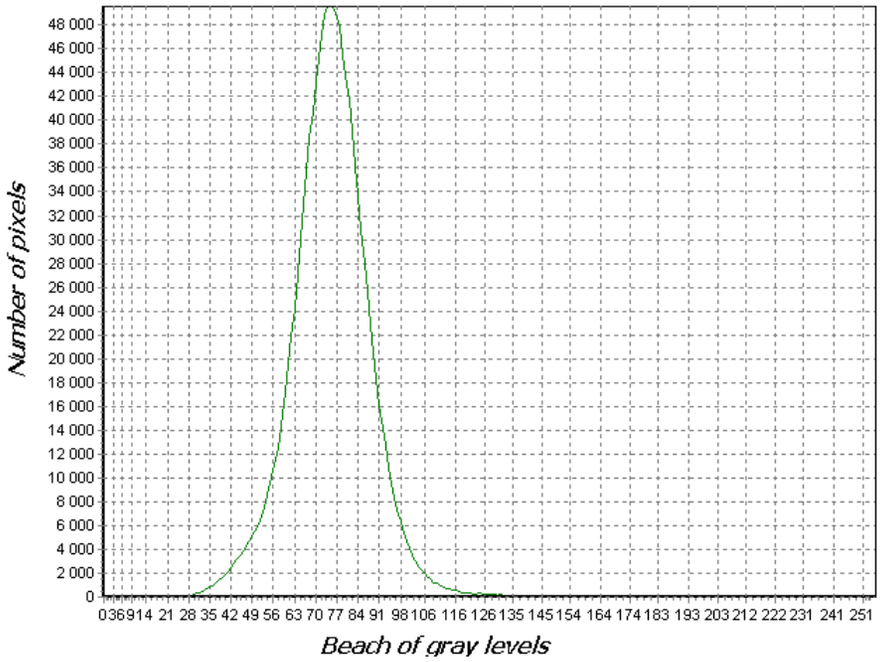

Figure 11. Signature of the filtered image illustrating the appearance of a polynomial function approximation by the least squares sense.

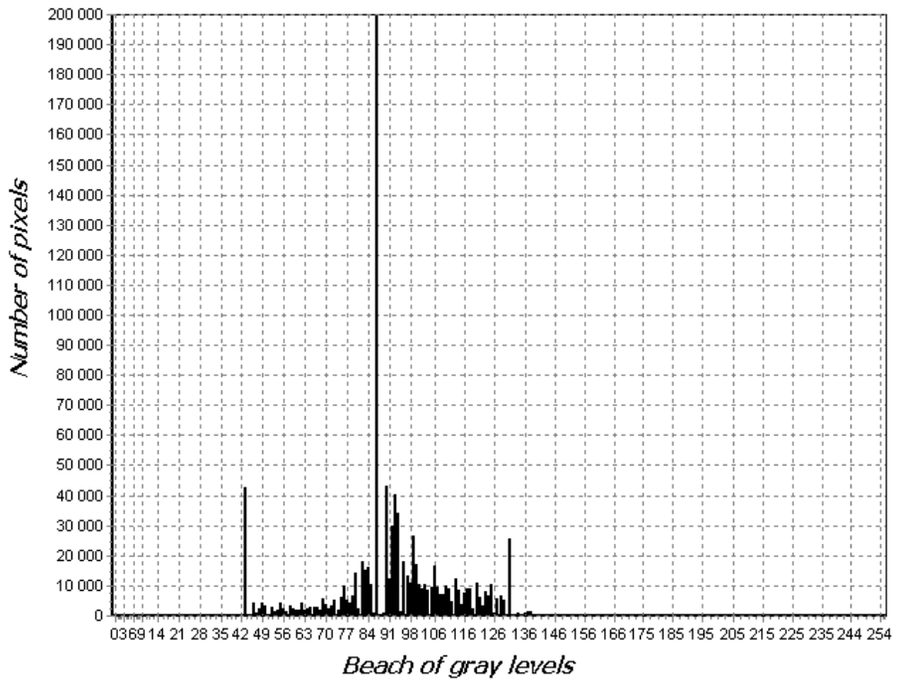

Figure 12. Texture image histogram obtained by index parameter of Haralick "Mean" on the Mount Cameroon region

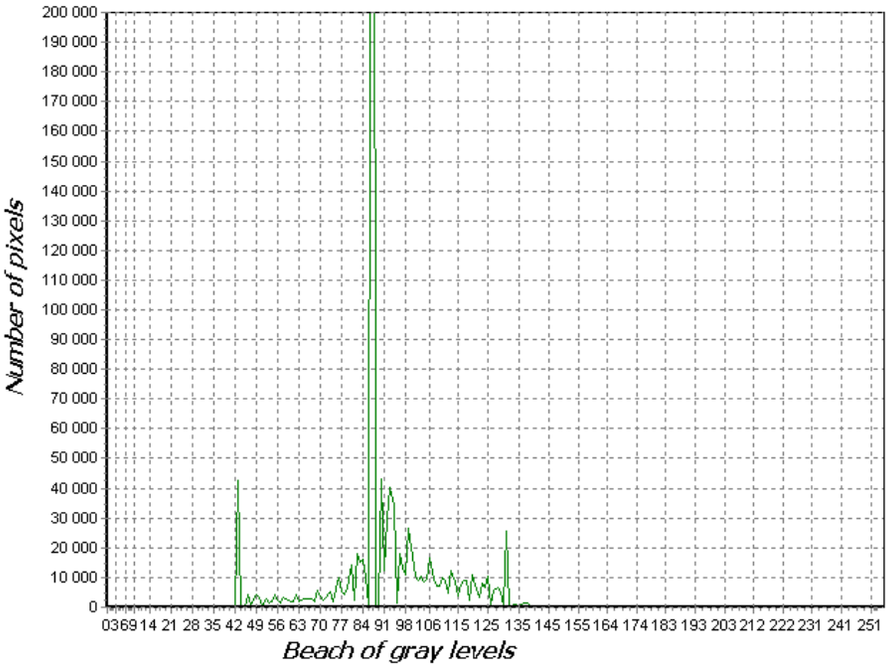

Figure 13. Corresponding signature of the texture image histogram

The image texture enhances the visual interpretation. Indeed, it contains information on the spatial distribution of color variations. This is observed in the texture image by the presence of dark shades, clear, smooth and gray. The texture image obtained does not allow partitioning of the image into separate classes because its histogram (Figure 7 or 11) does not present specific modes and valleys. It is again transformed using the histogram. This second representation offers the advantage of facilitating the visualization of local maxima and minima. Each representation has them peculiarities and shortcomings; however, the combined use of two methods of representation facilitates the detection thresholds for classification (Tables 2 and 3).

Table 3 shows the modes and valleys that were used in classification thresholds. It was obtained following the same methodological approach followed with the image data of the mangrove area.

	Thresholds / Color codes			
Modes	43	87	99	131
Color codes				
Valleys	55	90	97	103
Color codes				

Table 3. Detection thresholds for classification and color coding of thematic classes: case of Mount Cameroon region

5.3. Results of thematic maps

5.3.1. Case of mangrove region

The final classified image presents the results of unsupervised classification obtained with different thresholds identified above (Table 2). This result is obtained on the basis of 14 cluster centers. Thus, the classified image traces an occupancy map of the study site highlighting 14 thematic classes whose characterization using data from field missions, old maps and the lithographic charts, aerial photographs allowed us to establish different classes of information. The exploitation of these data led to the realization of the space map shown in figure 14.

Detecting the number of class by this approach remains a major challenge. However, after several experiments, we found that we could not indefinitely increase the number of classes. Indeed, it proved that beyond a certain value (14 in this case) noted almost no more change the final result. Moreover, for low numbers of classes, there was more of a smoothing of the final result with a merging of small units in large.

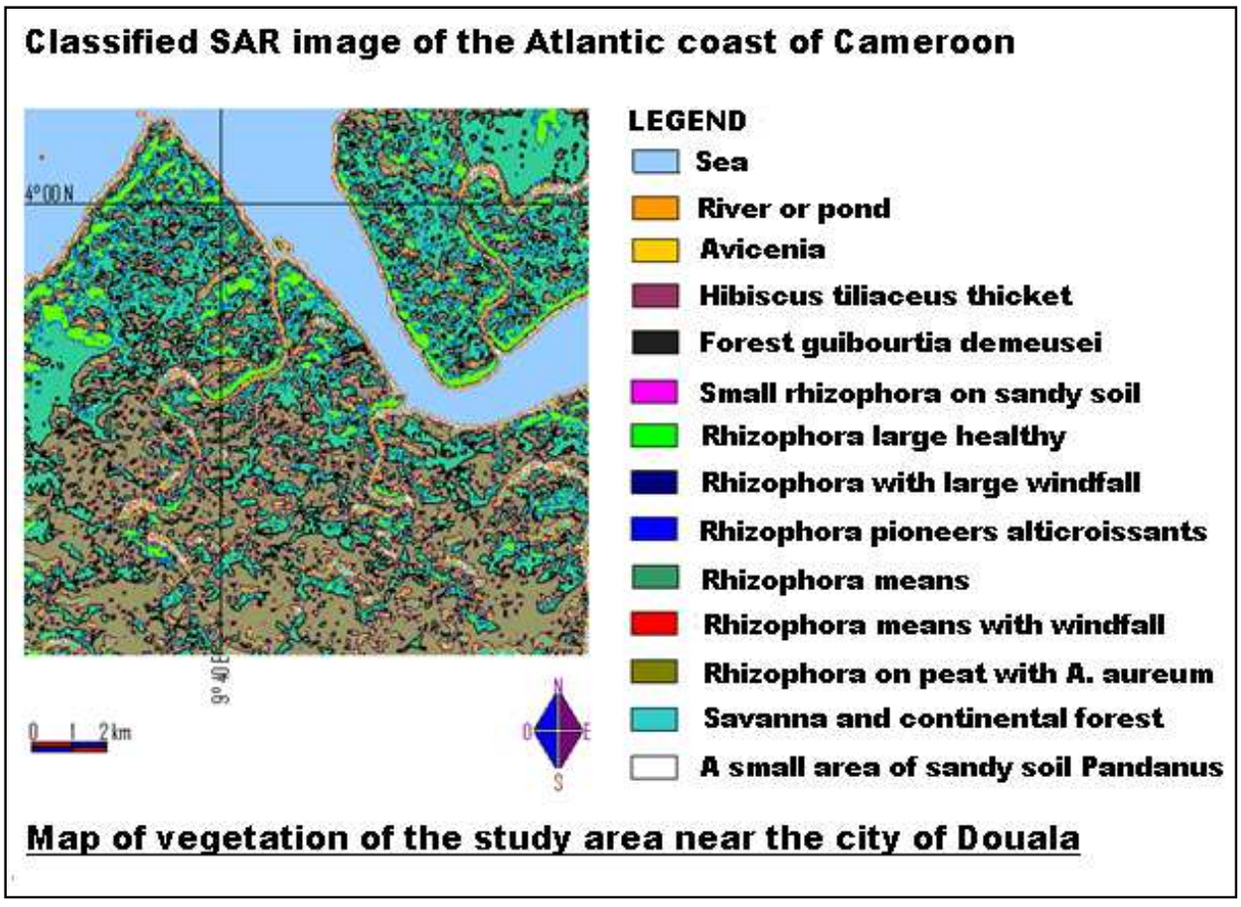

Figure 14. Satellite map from the mangrove region of the estuary of Douala, Cameroon

The classified image obtained from the 14 threshold and observing the color code (Table 2) is shown in Figure 14. This classification method belongs to the family of unsupervised classification. Indeed, the spectral classes are first formed. These classes are based solely on digital information data. As a result, the classification algorithm presents below is used to

determine statistical natural groups of data. We obtain quite detailed thematic classes. The 14 classes provide a map of land of the study site with good delineation of the different classes (Figure 14).

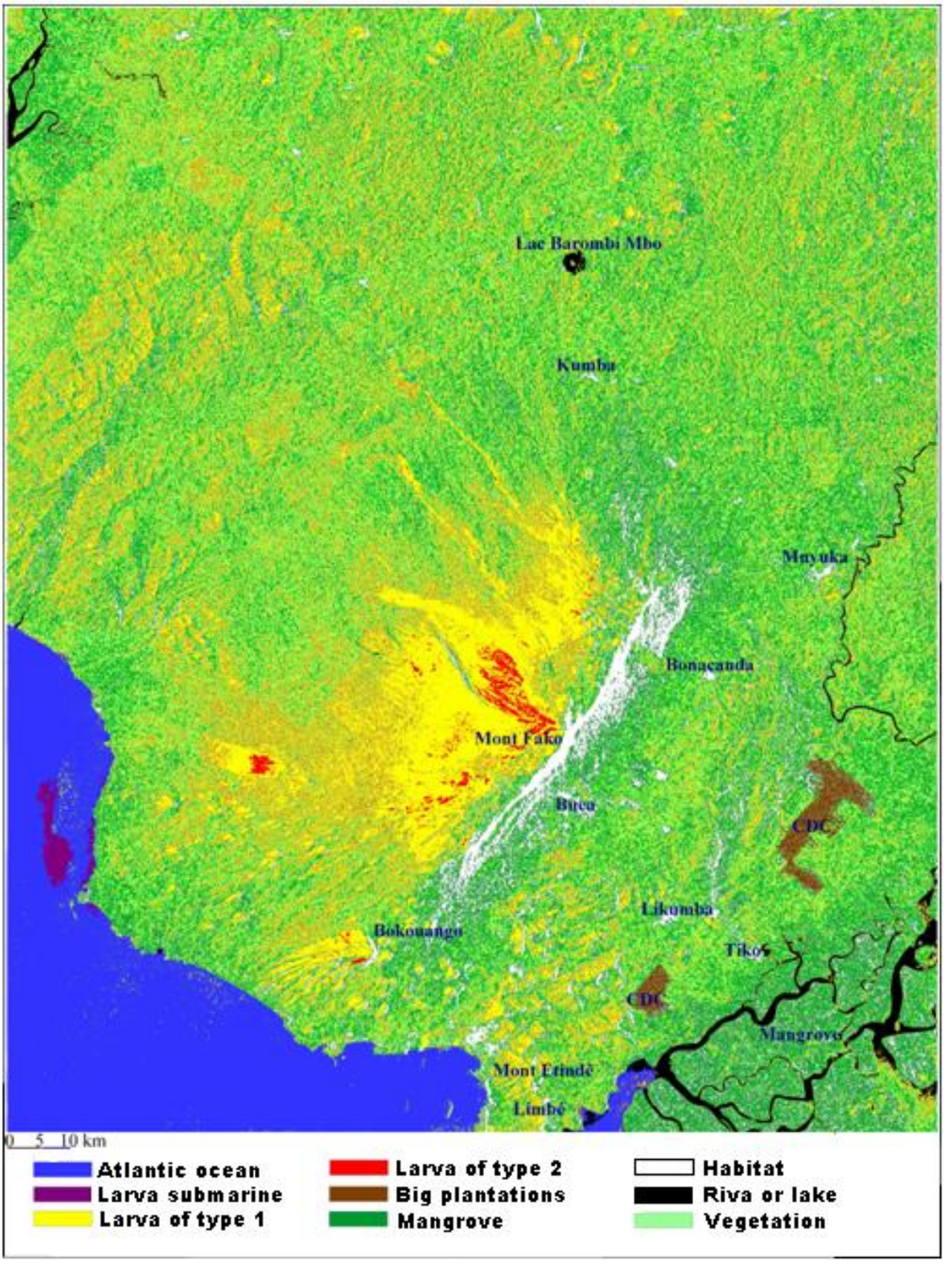

Figure 15. Satellite map from the Mount Cameroon region

Thematic classes are categories of interest that the analyst tries to identify in the images, as different types of crops, forests or species of trees, different types of rocks or geological features, etc.

The result obtained in this study presents a double advantage. The first advantage is at the level of accuracy in the identification of certain classes of information like the class sea. The second one is in the identification of certain thematic classes within certain classes of information and therefore a precise characterization can help in highlighting other information, as for example, different canopies in terms of vegetation class information.

5.3.2. Case of mount Cameroon region

In Figures 10 and 11, we have uni-modal aspect of the histogram of the image after filtering. This makes difficult any exploitation for segmentation. To overcome this drawback, it then uses to texture images.

Figures 12 and 13 show them with now m-modal shape observed on the histogram of the image texture. After several experiments, we retained eight cluster centers summarized in table 3 with the color codes used for each class center.

For the Mount Cameroon region, the same approach as that used previously on the mangrove is applied and the result is presented on Figure 15. The use of maps available and research work on this site (Akono et al., 2005, 2006) are used to characterize the eight thematic classes. The use of this information provides the classified image of the Mount Cameroon region including the specification of each class of information is summarized on the legend of Figure 15. As can be seen at the legend, we have nine more thematic classes instead of eight. This is because when classifying all pixels are not classified. All unclassified pixels were grouped in class vegetation. Furthermore, a broad thematic class (e.g. forest) may contain multiple spectral classes with spectral variations. Using the example of the forest, the spectral sub-classes can be caused by variations in age, species, tree density or simply the effects of shadowing or variations in illumination. The analyst's job is to determine the usefulness of different thematic classes and their correspondence to the thematic classes useful.

6. Conclusion

The purpose of this study was the production of space maps with the synthetic aperture radar (SAR) images. To achieve this, we proceed by adopting approaches optimized of texture analysis of images, using the statistical parameters of Haralick generalized at the order n. The approach is based on the concept of generic tree. It has the advantage of being less time consuming calculation from the conventional approach which frequently uses co-occurrence matrices for texture analysis and especially the processed images are generally very large sizes. In classification, the approach relies on the concept of detecting "modes" and "valleys" of histograms in a SAR image using classification of type unsupervised. For each of the SAR images, the histogram of the convolution image obtained at base of texture parameter is represented and approximated by a regression line called "signature" using

least square method. The operation of the histogram and the signature of the texture image can facilitate the detection of classification thresholds. The main interest of the proposed approach is that we have results that are approaching the best of the reality field; it also does not require a serial multi-date SAR data for the realization of satellite image maps. The method was successfully tested on two satellite images from two different sensors: one from the ESAR program obtained at the resolution 6m and one other from the ERS-1 sensor of resolution 25 m.

A limitation of the classification approach lies at the empirical detection of local extrema. A perspective would then be to automate the detection of the number of classes and local extrema.

Author details

Janvier Fotsing
Corresponding Author
University of Buea, Faculty of Science/Department of Physics, Cameroon

Emmanuel Tonye
University of Yaounde I, National Advanced School of Engineering, Department of Electrical and Telecommunications Engineering, Cameroon

Bernard Essimbi Zobo
University of Yaounde I, Faculty of Science, Department of Physics, Cameroon

Narcisse Talla Tankam
University of Dschang, Fotso Victor Institute of Technology, Department of Computer Sciences, Cameroon

Jean-Paul Rudant
University of Marne-La-Vallée, Institut Francilien des Géosciences, France

Acknowledgement

This work was supported by the LETS laboratory of the National Advanced School of Engineering of the University of Yaoundé I. We are also grateful unto the European Spatial Agency (ESA) for the grant of SAR ERS-1 image used in this study.

7. References

Akono, A.; Tonyé, E.; Ndi Nyoungui, A. (2003). Nouvelle méthodologie d'évaluation des paramètres de texture d'ordre trois. *Internationnal Journal of Remote Sensing*, vol.24, n°9, pp. 1957-1967.

Akono, A.; Talla Tankam, N.; Tonyé, E.; Dzepa, C. (2005). Nouvel algorithme d'évaluation des paramètres de texture d'ordre n sur la classification de l'occupation des sols de la région volcanique du Mont Cameroun. *Télédétection*, vol. 5, n° 1-2-3, pp. 227-244, Avril 2005.

Akono, A.; Talla Tankam, N.; Tonyé E.; Ndi Nyoungui, A.; Dipanda, A. (2006). High Order Textural Classification of two SAR ERS images on Mount Cameroon. *Geocarto International*, vol. 21, n° 3, pp.1-16.

Baltzer, F.; Rudant, J.-P.; Tonyé, E. (1996). Applications de la télédétection micro-ondes en bande C à la cartographie des mangroves de la région de Douala. *Proceedings of the second ERS applications Workshop*, ESA SP 383, pp. 455-461.

Bhattacharya, C., G. (1967). A simple method of resolution of a distribution into gaussian components. *Biometrics*, vol. 23, pp.115-135.

Caloz, R.; Collet, C. (2001). *Précis de télédétection, traitements numériques d'images de télédétection* (Presses de l'Université du Québec / AUF, Québec). Vol.3, 386 pages.

Cocquerez, J. -P.; Philipp, S.; Maître, H. (2001). *Analyse d'images: filtrage et segmentation* (Masson). Paris, Milan, Barcelonne.

Diday, E.; Lemaire, J.; Pouget, J.; Testu, F. (1982). *Elements d'analyse de données* (Dunod, Paris).

Fotsing, J.; Tonyé, E.; Talla Tankam, N.; Kanaa, T., F., N.; Rudant, J.-P. (2008). Classification non supervisée d'image RSO à l'aide d'extremums locaux d'histogramme: application à la cartographie de la mangrove littorale camerounaise. *Revue Française de la Photogrammétrie et de Télédétection*, vol. 1, n°189, pp. 28-39.

Franklin, S., E; Peddle, R., D. (1989). Spectral texture for improved class discrimination in complex terrain. *International Journal of Remote Sensing*, vol. 10 n°8, pp. 1437-1443.

Girard, M-C. (2004). *Traitement des données de télédétection* (Dunod). 530 pages.

Haralick, R., M.; Shanmugam, K.; Dinstein, I. (1973). Textural features for image classification. *IEEE Transactions on Systems, Man and Cybernetics*, vol. 3, nº 6, pp. 610 - 621.

Haralick R., M. (1979). Statistical and structural approaches to texture. *Proceedings of the IEEE*, vol. 67, n°5, pp. 786-804.

Jukka, H.; Aristide, V. (1998). Land cover/land use classification of urban areas: a remote sensing approach. *Internationnal Journal of Pattern Recognition and Artificial Intelligence.* Vol.12, n°4, pp. 475-489.

Kourgli, A.; Belhadj-Aissa, A. (1999). Nouvel algorithme de calcul des paramètres de texture appliqué à la classification d'images satellitaires. *Acte des 8 èmes Journées Scientifiques du Réseau Télédétection l'AUF.* Pp. 109-118, Lausanne, Suisse, 22-25 novembre 1999,. Ed. AUPELF-UREF, Analyse critique et perspectives. ISBN 2-920021-92-3.

Kourgly, A.; Belhadj-Aissa, A. (2003). Segmentation texturale des images urbaines par le biais de l'analyse variographique. *Revue Télédétection*, vol. 3, n° 2-3-4, pp. 337–348.

Lee, J.,S. (1981). Speckle analysis and smoothing of synthetic aperture radar images. *Computer Graphics and Image Processing*, vol. 17, pp. 24-32.

Li, W. (1994). Vector choice in the texture spectrum approach. *International Journal of Remote Sensing*, vol. 15, n°18, pp. 3823-3829.

Linders, J. (2000). Comparison of three different methods to select feature for discriminating forest cover types using SAR imagery. *International Journal of Remote Sensing*, vol. 21, nº 10, pp. 2089 - 2099.

Lorette, A. (1999). Analyse de texture par méthodes markoviennes et par morphologie mathématique: application à l'analyse des zones urbaines sur des images satellitales.

Thèse présentée à l'Université de Nice- Sophia Antipolis pour obtenir le titre de Docteur en Sciences Spécialité Sciences de l'Ingénieur. 162 pages.

Lucieer, A.; Stein, A.; Fisher, P. (2005). Multivariate texture-based segmentation of remotely sensed imagery for extraction of objects and their uncertainty. *International Journal of Remote Sensing*, vol. 26, nº 14, p. 2917 - 2936.

Marceau, D.,J.; Howarth, P., J.; Dubois, J-M., M.; Gratton, D., J. (1990). Evaluation of the gray-level co-occurrence matrix method for land-cover classification using SPOT imagery. *IEEE Transactions on Geoscience and Remote Sensing*, vol. 28, n° 4, pp. 513-518.

Oliver, C., J. (1993). Optimum texture estimators for SAR clutter. *Journal of Physics D: Applied Physics*, vol. 26, pp. 1824 - 1835.

Otsu, N. (1979). A threshold selection method from gray-level histograms. *IEEE Trans. On SMC*, vol.11, pp. 191-204.

Peckinpaugh, S., H. (1991). An improved method for computing gray-level co-occurrence matrix based texture measures. *Graphical models and Image Processing*, vol.53, pp. 574-580.

Pratt, W. (1991). *Digital image processing* (2nd edition, Willey-interscience). 698 pages.

Puissant, A.; Hirsch, J.; Weber, C. (2005). The utility of texture analysis to improve per-pixel classification for high to very high spatial resolution imagery. *International Journal of Remote Sensing*, vol. 26, nº 4, p. 733 - 745.

Randen, T.; Husoy, J., H. (1999). Filtering for texture classification: a comparative study. *IEEE Transactions PAMI*, vol. 21, nº 4, pp. 291-310.

Reed, T., R.; Hans Du Buf, J., M. (1993). A review of recent texture segmentation and feature extraction techniques. *CVGIP: Image Understanding*, vol. 57, n° 3, pp. 359-372.

Rudant, J-.P.; Baltzer, F.; Tupin, F.; Tonyé, E. (1997). Distinction entre formations végétales littorales et continentales dans leur rapport avec la géomorphologie: intérêt des images ERS-1. *Symposium ERS-1, Publications ESA*, pp. 1069-1073, Florence, 14-21 mars 1997.

Talla Tankam, N. (2003). Nouvelle méthodologie d'évaluation des paramètres de texture d'ordre n>1: Application aux images radar du Mont Cameroun. *Mémoire de DEA*, Université de Yaoundé I (Cameroun), 60 pages.

Talla Tankam, N.; Dipanda, A.; Tonyé, E.; Akono, A. (2006a). Classification d'images satellitaires radars RSO par valeurs propres de texture. Application à la mangrove littorale Camerounaise. *Actes du Colloque Africain sur la Recherche en Informatique (CARI'06)*, Cotonou (Bénin), 6-9 novembre 2006.

Talla Tankam, N.; Kouamé Koffi, F.; Dipanda, A.; Akono, A.; Bernier, M.; Tonyé, E.; Affian, K. (2006b). Caractérisation des discontinuités-images par l'approche de vecteur de texture: application à des images RSO d'ERS-2. *Journal des Sciences pour Ingénieurs (JSPI)*, n° 7, ISSN 0851-4453.

Talla Tankam, N. (2008). Une nouvelle approche d'analyse automatique de texture d'images : application à l'étude de la dynamique d'occupation spatiale sur le Mont Cameroun et ses environs. *Cotutelle de thèse de Doctorat/PhD en Informatique*, Université de Yaoundé I, Cameroun et l'Université de Bourgogne, France, 194 pages.

Ulaby F., T.; Kouyate, F.; Brisco, B.; Lee Williams T., H. (1986). Textural information in SAR images. *IEEE trans. Geosci. Remote Sens.* GE-24, pp. 235-245.

Unser, M. (1995). Texture classification and segmentation using wavelet frames. *IEEE Trans. On Image Processing*, vol. 4, n°11, pp. 1549-1560.